

# ESVM : An Open-source Electrostatic Vlasov-Maxwell Code

Michaël J TOUATI<sup>1, 2, 3</sup>

<sup>1</sup> Department of Electrical Engineering, University of California Los Angeles, Los Angeles, CA 90095, USA <sup>2</sup> Group of Lasers and Plasmas, IPFN, IST, Universidade de Lisboa, Lisbon, Portugal <sup>3</sup> Centro de Láseres Pulsados de Salamanca (CLPU), Edificio M5, Parque Científico, C/ Adaja 8, 37185 Villamayor, Salamanca, Spain (current affiliation)

DOI: [10.21105/joss.0XXXX](https://doi.org/10.21105/joss.0XXXX)

## Software

- [Review](#) ↗
- [Repository](#) ↗
- [Archive](#) ↗

Editor: [Editor Name](#) ↗

Submitted: 01 January XXXX

Published: 01 January XXXX

## License

Authors of papers retain copyright and release the work under a Creative Commons Attribution 4.0 International License ([CC BY 4.0](#)).

## Summary

ESVM (ElectroStatic Vlasov-Maxwell) is a single species 1D-1V Vlasov-Maxwell Fortran 90 code parallelized with OpenMP that allows for the study of collisionless plasmas. Many finite volume numerical advection schemes (Godunov, 1959) are implemented in the code in order to discretize the Vlasov equation, namely : - the donor-cell scheme i.e. the downwind / upwind scheme (R. Courant et al., 1952) depending on the advection direction in each phase-space cell, - the Lax-Wendroff scheme (Lax & Wendroff, 1960), - the Fromm scheme (Fromm, 1968), - the Beam-Warming scheme (Beam & Warming, 1976), - the Van Leer scheme (Van Leer, 1977), - the minmod scheme (Roe, 1986), - the superbee scheme (Roe, 1986) and - two Monotonic Upwind-centered Scheme for Conservation Laws (MUSCL) (van Leer, 1979) schemes MUSCL2 (Crouseilles & Filbet, 2004) and MUSCL1 (Duclos et al., 2009).

Contrary to the linear second order Lax-Wendroff, Fromm and Beam-Warming schemes, the non-linear second order minmod, superbee, Van Leer and MUSCL schemes make use of a Total Variation Diminishing (TVD) non-linear flux limiter with the price of becoming a first order scheme in some phase-space cells to limit the numerical oscillations. The donor-cell scheme is a first order method and has the pros of limiting such eventual oscillations but the cons of being numerically less consistent and more diffusive too. In ESVM, the discretized Vlasov equation is coupled with the self-consistent Maxwell-Gauss equation or equivalently with the Maxwell-Ampere equation with Maxwell-Gauss equation computed at the first time step, only. While the second order Maxwell-Gauss solver needs a computationally expensive inversion of a tridiagonal matrix for the computation of the Poisson equation, the Maxwell-Ampere equation solver makes use of the faster second order finite difference Yee scheme (Yee, 1966). Both absorbing and periodic boundary conditions for both the particles and the fields are implemented. Python scripts, using the Matplotlib and Numpy packages, are provided to automatically extract and plot the stored simulation results. Compilation rules can be easily modified depending on the user compiler preferences using the provided makefile. It is however recommended to compile the code using the double-precision compiler option. Well known Plasma Physics academic cases, tools for testing the compilation and tools for checking the simulation parameters that are specified by the user in the input-deck are provided.

## Statement of need

ESVM has been developed in order to adapt simulations to specific Plasma Physics problems by choosing the more adequate finite volume numerical advection scheme in order to compute the Vlasov equation phase-space advection derivatives and to choose between computing the

Maxwell-Gauss equation or the Maxwell-Ampere equation with Maxwell-Gauss equation computed at the first time step, only. The code aims at being used by the open-source Highly Parallel Computing (HPC) Plasma Physics community ranging from under or post-graduate students to teachers and researchers who usually use Particle-In-Cell (PIC) codes (Dawson, 1962) to study collisionless plasmas. Indeed, the PIC method may prohibit the study of Plasma Physical processes on large time scales and/or for very dense collisionless plasmas due to the statistical and numerical fluctuations of the computed quantities imposed by the use of a finite number of macroparticles. Also, plasma instabilities naturally develop in PIC codes, seeded by the available fluctuations spatial spectrum  $k$ -vector for which the instability growth rate is maximum and some small amplitude Plasma Physical processes may be hidden under the fluctuations level. Compared to the many open source PIC code such as (Derouillat et al., 2018) and semi-Lagrangian codes such as (de Buyl, 2014), there is no open source finite volume Vlasov codes in the literature that are not based on an expansion method such as (Tzoufras et al., 2011) (Touati et al., 2014) or (Joglekar & Levy, 2020). In addition, since the Vlasov equation is a conservation equation of the number of particle in the phase-space, using a finite volume method in order to compute the Vlasov equation presents the advantage of allowing for the use of numerical schemes that are numerically flux conserving and/or that ensure the distribution function positivity compared to other numerical methods. ESVM has already been used during courses for under and post-graduate students about the “numerical tools for laser-plasma interaction Physics” and it is currently used for theoretical Plasma Physics investigations.

## Equations computed by ESVM

Plasma ions are assumed to be immobile with a homogeneous density  $n_i$  and fully ionized with an electrical charge  $Ze$  where  $Z$  is the plasma ion atomic number and  $e$  the elementary charge. The plasma electron distribution function  $f_e(x, v_x, t)$  is computed by ESVM according to the plasma electron Vlasov equation

$$\frac{\partial f_e}{\partial t}(x, v_x, t) + \frac{\partial}{\partial x}(v_x f_e(x, v_x, t)) - \frac{\partial}{\partial v_x} \left( \frac{e}{m_e} E_x(x, t) f_e(x, v_x, t) \right) = 0 \quad (1)$$

that is self-consistently coupled with the Maxwell-Gauss equation

$$\frac{\partial E_x}{\partial x}(x, t) = 4\pi e (Zn_i - n_e(x, t)) \quad (2)$$

for the electrostatic field  $E_x(x, t)$  or, equivalently, self-consistently coupled with the Maxwell-Ampere equation

$$\frac{\partial E_x}{\partial t}(x, t) = -4\pi j_e(x, t) \quad (3)$$

with Maxwell-Gauss equation Equation 2 computed at the simulation start  $t = 0$ , only. Indeed, by integrating the plasma electron Vlasov equation Equation 1 over the whole plasma electron velocity space  $v_x \in [v_{x,\min}, v_{x,\max}]$ , one gets the hydrodynamic equation of plasma electron number conservation

$$\frac{\partial n_e}{\partial t}(x, t) + \frac{\partial}{\partial x}(n_e v_e(x, t)) = 0, \quad (4)$$

which, when injected in the time derivative of Maxwell-Gauss equation Equation 2, provides the Maxwell-Ampere equation Equation 3 if Maxwell-Gauss equation Equation 2 is verified at the simulation start  $t=0$ . Here,

$$n_e(x, t) = \int_{v_{x,\min}}^{v_{x,\max}} f_e(x, v_x, t) dv_x, \quad (5)$$

$$v_e(x, t) = \frac{1}{n_e(x, t)} \int_{v_{x,\min}}^{v_{x,\max}} f_e(x, v_x, t) v_x dv_x \quad (6)$$

78 and

$$j_e(x, t) = -en_e(x, t)v_e(x, t) \quad (7)$$

79 are the plasma electron density, mean velocity and electrical charge current, respectively.  
80 ESVM also computes the plasma electron thermal velocity  $v_{T_e}(x, t)$  defined according to the  
81 plasma electron internal energy density

$$u_{T_e}(x, t) = \frac{n_e(x, t)}{2} m_e v_{T_e}(x, t)^2 = \frac{m_e}{2} \int_{v_{x, \min}}^{v_{x, \max}} f_e(x, v_x, t) (v_x - v_e(x, t))^2 dv_x. \quad (8)$$

82 For example, in 1D plasmas at local Maxwell-Boltzmann equilibrium,  $v_{T_e}(x, t) =$   
83  $\sqrt{k_B T_e(x, t)/m_e}$  where  $k_B$  is the Boltzmann constant,  $T_e(x, t)$  is the local electron  
84 temperature and  $m_e$  the electron mass. Maxwell-Gauss equation Equation 2 is computed by  
85 using the electrostatic potential definition

$$\frac{\partial \Phi}{\partial x}(x, t) = -E_x(x, t) \quad (9)$$

86 that gives the Poisson equation

$$\frac{\partial^2 \Phi}{\partial x^2}(x, t) = -4\pi e (Zn_i - n_e(x, t)) \quad (10)$$

87 for the electrostatic potential  $\Phi$  when injected in the Maxwell-Gauss equation Equation 2.  
88 When the simulation is running, ESVM stores at every time steps and displays on the terminal  
89 at every dumped time steps  $t_d$  the total plasma electron internal and kinetic energy (assuming  
90 simulations with an area unit perpendicular to the  $x$ -axis of  $\lambda_{\text{Debye}}^2$ ) and the total electrostatic  
91 energy in the simulation box  $x \in [x_{\min}, x_{\max}]$

$$U_{T_e}(t_d) = \lambda_{\text{Debye}}^2 \int_{x_{\min}}^{x_{\max}} u_{T_e}(x, t_d) dx, \quad (11)$$

$$U_{K_e}(t_d) = \lambda_{\text{Debye}}^2 \int_{x_{\min}}^{x_{\max}} n_e(x, t) \frac{m_e v_e(x, t_d)^2}{2} dx \quad (12)$$

93 and

$$U_{E_x}(t_d) = \lambda_{\text{Debye}}^2 \int_{x_{\min}}^{x_{\max}} \frac{E_x(x, t_d)^2}{8\pi} dx, \quad (13)$$

94 respectively as well as the total energy area density

$$U_{\text{tot}}(t_d) = U_{T_e}(t_d) + U_{K_e}(t_d) + U_{E_x}(t_d) \quad (14)$$

95 in order to check the energy conservation in the simulation. The user can initialize : - an  
96 initial plasma electron population at Maxwell-Boltzmann equilibrium drifting at the velocity  $v_d$

97

$$\begin{cases} f_e(x, v_x, t=0) &= \frac{Zn_i}{\sqrt{2\pi v_{T_{e0}}^2}} \exp\left[-\frac{(v_x - v_d)^2}{2v_{T_{e0}}^2}\right] \\ E_x(x, t=0) &= 0 \end{cases} \quad (15)$$

98 by no imposing any perturbation parameter or - a well known Plasma Physics process;  
99 cf. section **ESVM Plasma Physics academic case simulations**. - Finally, specific Plasma  
100 Physics simulations can easily be added in ESVM by implementing them in the Fortran 90  
101 subroutine INIT\_SIMU of the library.f90 source file.

## ESVM units

The code units consist in the commonly used electrostatic units : the electron mass  $m_e$  for masses, the elementary charge  $e$  for electrical charges, the inverse of the Langmuir plasma electron angular frequency  $\omega_p = \sqrt{4\pi Z n_i e^2 / m_e}$  for times, the Debye electron screening length  $\lambda_{\text{Debye}} = v_{T_{e0}} / \omega_p$  and the constant electron density  $n_0 = Z n_i$  for spatial densities.  $v_{T_{e0}}$  is therefore an important unit parameter of normalization since it fixes indirectly the space unit. It can be defined more generally as the initial plasma electron velocity distribution standard deviation if the plasma is not initialized at Maxwell-Boltzmann thermodynamic equilibrium; cf. Equation 8. Injecting these units in the equations computed by the code, one deduces the resulting normalized electrostatic field and electron distribution function that consequently reads  $\underline{E}_x = e E_x / m_e \omega_p v_{T_{e0}}$  and  $\underline{f}_e = f_e v_{T_{e0}} / n_0$ , respectively.

## ESVM numerical stability

The spatial grid cells should be chosen lower than the Debye length  $\Delta x < \lambda_{\text{Debye}}$  for the simulation to be Physical.  $v_{x,\min}$  and  $v_{x,\max}$  should be chosen sufficiently large  $|v_{x,\min/\max}| \gg v_{T_{e0}}$  in such a way that there is no plasma electrons outside the simulation velocity space during the whole simulation. The simulation velocity bin size should be chosen lower than the thermal electron velocity  $\Delta v_x < v_{T_{e0}}$  and also sufficiently small to capture the desired Physics. The CFL stability condition (from the name of its finder R. Courant, K. Friedrichs and H. Lewy (R. Courant et al., 1928)) is implemented inside the code in such a way that the user just needs to specify in the input deck the scalar parameter  $\text{cfl} < 1$  such that the normalized simulation time step reads

$$\Delta t_n = \text{cfl} \times F^n(\Delta x, \Delta v_x) < F^n(\Delta x, \Delta v_x) \quad (16)$$

at the time step  $t_n = \sum_{m=1}^n \Delta t_m$  at time iteration  $n$  where  $F^n(\Delta x, \Delta v_x)$  depends on the chosen numerical scheme.

For example, if one notes

$$\underline{f}_e^{n,i} = \frac{1}{\Delta x} \int_{\underline{x}_{i-1/2}}^{\underline{x}_{i+1/2}} \underline{f}_e(\underline{x}, t_n) d\underline{x} \quad (17)$$

the electron distribution function finite volume at the spatial location  $\underline{x}_i$  located in between  $\underline{x}_{i-1/2} = \underline{x}_i - \Delta x/2$  and  $\underline{x}_{i+1/2} = \underline{x}_i + \Delta x/2$  and one considers the Lax-Wendroff method to compute the advection

$$\frac{\partial \underline{f}_e}{\partial t} + \underline{v}_x \frac{\partial \underline{f}_e}{\partial \underline{x}} = 0 \quad (18)$$

of plasma electrons along the spatial  $\underline{x}$ -axis in the phase-space, the numerical scheme reads

$$\left[ \frac{\underline{f}_e^{n+1} - \underline{f}_e^n}{\Delta t_n} \right]^i + \underline{v}_x \left[ \frac{\underline{F}_x^{i+1/2} - \underline{F}_x^{i-1/2}}{\Delta x} \right]^n = 0 \quad (19)$$

where the plasma electron fluxes across the volume sections located at  $\underline{x}_{i\pm 1/2}$  are given by

$$\underline{F}_x^{n,i+1/2} = \frac{\underline{f}_e^{n,i+1} + \underline{f}_e^{n,i}}{2} - \frac{\underline{v}_x \Delta t_n}{\Delta x} \frac{\underline{f}_e^{n,i+1} - \underline{f}_e^{n,i}}{2} \quad (20)$$

and

$$\underline{F}_x^{n,i-1/2} = \frac{\underline{f}_e^{n,i} + \underline{f}_e^{n,i-1}}{2} - \frac{\underline{v}_x \Delta t_n}{\Delta x} \frac{\underline{f}_e^{n,i} - \underline{f}_e^{n,i-1}}{2}. \quad (21)$$

132 According to the Taylor expansion of  $f_e^{n,i+i}$ ,  $f_e^{n,i-i}$  and  $f_e^{n+1,i}$  close to  $(\underline{x}_i, \underline{t}_n)$  up to the  
 133 third order in space and time, one can check the Lax-Wendroff numerical consistency error is  
 134 indeed of second order :

$$\begin{aligned} \epsilon^{n,i} &= \left[ \frac{f_e^{n+1} - f_e^n}{\Delta t_n} \right]^i + v_x \left[ \frac{F_x^{i+1/2} - F_x^{i-1/2}}{\Delta x} \right]^n - \left( \left. \frac{\partial f_e}{\partial t} \right|^{n,i} + v_x \left. \frac{\partial f_e}{\partial x} \right|^{n,i} \right) \\ &= \frac{\Delta t_n^2}{6} \left. \frac{\partial^3 f_e}{\partial t^3} \right|^{n,i} + \frac{v_x \Delta x^2}{6} \left. \frac{\partial^3 f_e}{\partial x^3} \right|^{n,i} + O(\Delta t_n^3 + \Delta x^3 + \Delta t_n \Delta x^2). \end{aligned} \quad (22)$$

135 By using the Von Neumann stability analysis, assuming periodic boundary conditions for  
 136 simplicity and noting

$$\hat{f}_e^n(\underline{k}^p) = \frac{1}{N_x} \sum_{i=1}^{N_x} f_e^{i,n} \exp(-i \underline{k}^p \underline{x}_i) \Leftrightarrow f_e^{n,i} = \sum_{p=1}^{N_x} \hat{f}_e^n(\underline{k}^p) \exp(i \underline{k}^p \underline{x}_i) \quad (23)$$

137 with  $i^2 = -1$ ,  $N_x = 1 + (x_{\max} - x_{\min})/\Delta x$  the number of spatial grid points and  $\underline{k}^p =$   
 138  $2\pi(p-1)/(x_{\max} - x_{\min})$  the discrete Fourier mode, one gets by injecting Equation 23 in  
 139 Equation 19

$$\frac{\hat{f}_e^{n+1}(\underline{k}^p)}{\hat{f}_e^n(\underline{k}^p)} = 1 - \frac{v_x \Delta t_n}{\Delta x} i \sin(\underline{k}^p \Delta x) + \left( \frac{v_x \Delta t_n}{\Delta x} \right)^2 [\cos(\underline{k}^p \Delta x) - 1] \quad (24)$$

140 for each term  $p$  of the series. It implies the numerical scheme is stable,

$$\text{meaning } \left| \frac{\hat{f}_e^{n+1}(\underline{k}^p)}{\hat{f}_e^n(\underline{k}^p)} \right| < 1, \text{ if } \Delta t_n < \frac{\Delta x}{v_x}. \quad (25)$$

141 Performing the same reasoning when discretizing also the velocity space  $v_x^\ell = v_{x,\min} + (\ell -$   
 142  $1)\Delta v_x$  with  $N_{v_x} = 1 + (v_{x,\max} - v_{x,\min})/\Delta v_x$  velocity grid points and considering in addition  
 143 the advection term of plasma electrons along the  $v_x$ -axis in the velocity space for computing  
 144 the Vlasov equation Equation 1 with each numerical scheme implemented in ESVM, one finds  
 145 (sometimes empirically when it is too difficult analytically) that

$$F^n(\Delta x, \Delta v_x) = \frac{1/2}{\frac{\max_{\ell \in [1, N_{v_x}]} \{v_x^\ell\}}{\Delta x} + \frac{\max_{i \in [1, N_x]} \{E_x^{n,i}\}}{\Delta v_x}}. \quad (26)$$

146 is a sufficient CFL stability condition for all numerical schemes implemented in ESVM to be  
 147 stable.

## 148 ESVM Plasma Physics academic case simulations

149 Four well-known Plasma Physics academic cases are provided with ESVM : 1) the emission of  
 150 an electrostatic wakefield by a Gaussian electron; cf. Figure 1 2) the linear Landau damping of  
 151 an electron plasma wave; cf. Figure 3, 3) the non-linear Landau damping of an electron plasma  
 152 wave; cf. Figure 2 and 4) the two-stream instability of two counter-propagating symmetric  
 153 Gaussian electron beams; cf. Figure 4.

154 For each academic case, an example of input deck is provided together with the corresponding  
 155 simulation result plots that the code typically generates. For 1), 2) and 3), the simulation is

156 initialized assuming a non-drifting collisionless plasma at Maxwell-Boltzmann equilibrium

$$\begin{cases} f_e^{(0)}(x, v_x, t = 0) &= \frac{Zn_i}{\sqrt{2\pi v_{Te_0}^2}} \exp\left[-\frac{v_x^2}{2v_{Te_0}^2}\right] \\ E_x^{(0)}(x, t = 0) &= 0 \end{cases} \quad (27)$$

157 that is perturbed : - with a small perturbation

$$\delta f_e(x, v_x, t = 0) = A \frac{Zn_i}{2\pi\delta x\delta v} \exp\left[-\frac{(x - x_d)^2}{2\delta x^2}\right] \exp\left[-\frac{(v_x - v_d)^2}{2\delta v^2}\right], \quad (28)$$

158 consisting in a Gaussian electron located at  $x_d = x_{\min} + (x_{\max} - x_{\min})/8$  with a standard  
159 deviation  $\delta x = \lambda_{\text{Debye}}/4$  and drifting at a velocity  $v_d$  with a standard deviation  $\delta v = v_{Te_0}/40$   
160 at the simulation start  $t = 0$  for 1), and - with a small perturbation consisting in a small  
161 amplitude electron plasma wave

$$\delta E_x(x, t < \delta t) = A \frac{m_e \omega_p v_{Te_0}}{e} \sin(\omega_0 t - kx) \quad (29)$$

162 propagating during a short time interval  $\delta t = 6\pi/\omega_0$  after the simulation start  $t = 0$  for 2)  
163 and 3).

164 Only the perturbation amplitudes  $A < 1$  for 1), 2) and 3), the perturbation drift velocity  
165  $v_d > v_{Te_0}$  for 1) and the perturbation temporal and spatial angular frequencies  $\omega_0$  and  $k$  for  
166 2) and 3) should be modified by the user when filling the input-deck in such a way that

$$\begin{cases} f_e(x, v_x, t) &= f_e^{(0)}(x, v_x, t) + \delta f_e(x, v_x, t) \\ E_x(x, t) &= E_x^{(0)}(x, t) + \delta E_x(x, t) \end{cases} \quad \text{with } |\delta f_e(x, v_x, t)| \ll f_e^{(0)}(x, v_x, t) \quad (30)$$

167 keeps being respected during the linear stage of the simulation. Except for non-linear Plasma  
168 Physics processes such as 3) for which the non-linear theory should be considered, the method-  
169 ology that can be used to check any ESVM simulation results is always the same. Only  
170 analytical estimates used to check the ESVM simulation results of the provided academic  
171 case 4) are consequently detailed here in order to highlight it. The user can check the  
172 provided academic case simulation results 1), 2) and 3) by directly comparing the ESVM sim-  
173 ulation results with the analytical estimates provided in (Decyk, 1987) (available at <https://picksc.idre.ucla.edu/wp-content/uploads/2015/04/DecykKyiv1987.pdf>) and in the refer-  
174 ence textbooks (Landau & Lifshitz, 1981) and (Sagdeev & Galeev, 1969), respectively.  
175

176 The provided Plasma Physics academic case 4) is initialized assuming two counter-propagating  
177 homogeneous Gaussian electron beams ' $e, +$ ' and ' $e, -$ ' of exactly opposite drift velocity  $\pm v_d$   
178 with same standard velocity deviation  $v_{Te_0}$

$$f_e^{(0)}(x, v_x, t) = f_{e,+}^{(0)}(x, v_x, t) + f_{e,-}^{(0)}(x, v_x, t) \quad (31)$$

179 with

$$f_{e,\pm}^{(0)}(x, v_x, t) = \frac{Zn_i/2}{\sqrt{2\pi v_{Te_0}^2}} \exp\left[-\frac{(v_x \mp v_d)^2}{2v_{Te_0}^2}\right] \quad (32)$$

180 that is a solution of the Vlasov Equation Equation 1 and that doesn't produce any electrostatic  
181 fields

$$E_x^{(0)}(x, t) = 0 \quad (33)$$

182 according to Maxwell-Gauss Equation Equation 2. If one computes the Vlasov-Maxwell set  
183 of Equations {Equation 1, Equation 2} exactly, initializing it with the two-stream equilibrium

184 distribution function Equation 31 without any perturbation, the counter-propagating elec-  
 185 tron beams would continue their propagation through the immobile plasma ions without any  
 186 modification. In order to observe the two-stream instability,

$$f_e(x, v_x, t = 0) = f_e^{(0)}(x, v_x, t = 0) + \delta f_e(x, v_x, t = 0), \quad (34)$$

187 is initialized instead by adding a small perturbation

$$\delta f_e(x, v_x, t = 0) = \delta f_{e,+}(x, v_x, t = 0) + \delta f_{e,-}(x, v_x, t = 0) \quad (35)$$

188 on each beam of the form

$$\delta f_{e,\pm}(x, v_x, t = 0) = \pm A \sin(k_1 x) f_{e,\pm}^{(0)}(x, v_x, t = 0) \quad (36)$$

189 at the simulation start  $t = 0$  with  $A = 0.1$ ,  $k_1 = 2\pi/L_x$  (parameter  $k$  in the input-deck)  
 190 where  $L_x = x_{\max} - x_{\min}$  can be modified by the user in the input-deck.

191 In order to get analytical estimates of growing plasma electron density and mean velocity and  
 192 electrostatic fields in this ESVM simulation, one can linearize the Vlasov equation Equation 1  
 193 and the self-consistent Maxwell-Gauss equation Equation 2 computed by ESVM assuming the  
 194 perturbation Equation 35 remains small compared to the equilibrium distribution Equation 31  
 195 during the simulation. They read

$$\frac{\partial \delta f_e}{\partial t} + \frac{\partial}{\partial x}(v_x \delta f_e) - \frac{e}{m_e} \frac{df_e^{(0)}}{dv_x} \delta E_x = 0 \quad (37)$$

196 and

$$\frac{\partial \delta E_x}{\partial x} = -4\pi e \int_{-\infty}^{\infty} \delta f_e dv_x, \quad (38)$$

197 up to the first order. Considering periodic boundary conditions, we may use a one-sided  
 198 Fourier transformation in time (thus equivalent to a Laplace transform) and a Fourier series  
 199 expansion in space for such a  $L_x$ -periodic initial condition problem. We will note

$$\hat{X}_p(t) = \frac{1}{L_x} \int_0^{L_x} X(x, t) \exp(+ik_p x) dx \Leftrightarrow X(x, t) = \sum_{p=-\infty}^{\infty} \hat{X}_p(t) \exp(-ik_p x) \quad (39)$$

200 with  $\forall p \in \mathbb{Z}$ ,  $k_p = 2\pi p/L_x$  and

$$\begin{aligned} \hat{\hat{X}}_p^{(+)}(\omega) &= \int_0^{\infty} dt \hat{X}_p(t) \exp(-i\omega t) \\ &= \int_0^{\infty} dt \int_0^{L_x} \frac{dx}{L_x} X(x, t) \exp[-i(\omega t - k_p x)] \\ \Leftrightarrow X(x, t) &= \int_{\iota R - \infty}^{\iota R + \infty} \frac{d\omega}{2\pi} \sum_{p=-\infty}^{\infty} \hat{\hat{X}}_p^{(+)}(\omega) \exp[+i(\omega t - k_p x)] \end{aligned} \quad (40)$$

201 where the integral in the complex  $\omega$ -plane is taken along a straight line  $\omega = \iota R$ . By multiplying  
 202 Equation 37 and Equation 38 by  $\exp[-i(\omega t - k_p x)]/L_x$  and by integrating them from  $x =$   
 203  $-\infty$  to  $x = \infty$  and from  $t = 0$  to  $t = \infty$ , we obtain respectively

$$\hat{\hat{f}}_{e,p}^{(+)} = \frac{1}{\iota(\omega - k_p v_x)} \left[ \hat{\hat{f}}_{e,p}(v_x, t = 0) + \frac{e}{m_e} \frac{df_e^{(0)}}{dv_x} \hat{\hat{E}}_{x,p}^{(+)} \right] \quad (41)$$

204 with

$$\hat{\hat{f}}_{e,p}(v_x, t = 0) = \alpha_p A \frac{Z n_i / 2}{\sqrt{2\pi v_{Te_0}^2}} \left\{ \exp\left[-\frac{(v_x - v_d)^2}{2v_{Te_0}^2}\right] - \exp\left[-\frac{(v_x + v_d)^2}{2v_{Te_0}^2}\right] \right\} \quad (42)$$



205 where

$$\alpha_p = \begin{cases} \mp 1/2\iota & \text{if } p = \pm 1 \\ 0 & \text{else} \end{cases} \quad (43)$$

206 and

$$\widehat{\widehat{\mathbf{E}}}_{x,p}^{(+)} = \frac{4\pi e}{\iota k_p} \int_{-\infty}^{\infty} \widehat{\mathbf{f}}_{e,p}^{(+)}(\omega, v_x) dv_x. \quad (44)$$

207 Injecting Equation 41 in Equation 44, we obtain the Fourier components of the electrostatic  
208 field Laplace transform

$$\begin{aligned} \widehat{\widehat{\mathbf{E}}}_{x,p}^{(+)}(\omega) &= \frac{4\pi e}{k_p^2 \epsilon(\omega, k_p)} \int_{-\infty}^{\infty} \frac{\widehat{\mathbf{f}}_{e,p}(v_x, t=0)}{v_x - \omega/k_p} dv_x \\ &= \alpha_p \frac{A}{2\sqrt{2}} \frac{m_e v_{Te0}}{e} \frac{\mathcal{Z}\left(\frac{\omega/k_p - v_d}{v_{Te0}\sqrt{2}}\right) - \mathcal{Z}\left(\frac{\omega/k_p + v_d}{v_{Te0}\sqrt{2}}\right)}{\epsilon(\omega, k_p) (k_p \lambda_{\text{Debye}})^2} \end{aligned} \quad (45)$$

209 where the plasma electrical permittivity reads

$$\begin{aligned} \epsilon(\omega, k) &= 1 - \frac{4\pi e^2}{m_e k^2} \int_{-\infty}^{\infty} \frac{1}{v_x - \omega/k} \frac{df_e^{(0)}}{dv_x} dv_x \\ &= 1 + \frac{1}{(k \lambda_{\text{Debye}})^2} \left\{ 1 + \frac{1}{2} \left[ F\left(\frac{\omega/k - v_d}{v_{Te0}\sqrt{2}}\right) + F\left(\frac{\omega/k + v_d}{v_{Te0}\sqrt{2}}\right) \right] \right\} \end{aligned} \quad (46)$$

210 depending on the plasma dispersion function (Fried & Conte, 1961)

$$F(\zeta) = \zeta \mathcal{Z}(\zeta) \text{ and } \mathcal{Z}(\zeta) = \frac{1}{\sqrt{\pi}} \int_{-\infty}^{\infty} \frac{\exp(-z^2)}{z - \zeta} dz. \quad (47)$$

211 Since  $v_d \gg v_{Te0}$  in this ESVM simulation, we have the condition

$$\left| \frac{\omega}{k_p} \pm v_d \right| \gg v_{Te0} \sqrt{2} \quad (48)$$

212 that is fulfilled for any given spatial frequency mode  $k_p$  and one thus may use the asymptotic  
213 limit

$$F(\zeta) \Big|_{|\zeta| \gg 1} = \iota \zeta \sqrt{\pi} \exp(-\zeta^2) - 1 - \frac{1}{2\zeta^2} - \frac{3}{4\zeta^4} + O\left(\frac{1}{\zeta^6}\right) \quad (49)$$

214 that leads to the simpler dispersion relation

$$\epsilon(\omega, k) \Big|_{v_d \gg v_{Te0}} = 1 - \frac{\omega_p^2}{2} \left[ \frac{1}{(\omega - kv_d)^2} + \frac{1}{(\omega + kv_d)^2} \right] = 0 \quad (50)$$

215 retaining only the main term in the series expansion of the dispersion function Equation 47  
216 up to the second order Equation 49. In this limit, the dispersion relation Equation 50 provides  
217 four pure real solutions  $\{\omega_1(k), \omega_2(k), \omega_3(k), \omega_4(k)\} \in \mathbb{R}^4$  for wavenumber  $k$  greater  
218 or equal than the critical wavenumber  $\omega_p/v_d$ . It means that the two counter-propagating  
219 electron beams remain stable on space scales smaller than  $2\pi v_d/\omega_p$ . However, in the case  
220 where  $k_p < \omega_p/v_d$  considered here, one finds in addition to the two real poles

$$\omega_{1/2}\left(k < \frac{\omega_p}{v_d}\right) = \pm \omega_0(k) \quad (51)$$

221 where

$$\omega_0(k) = \omega_p \sqrt{\left(\frac{kv_d}{\omega_p}\right)^2 + \frac{1}{2} \left(1 + \sqrt{1 + 8\left(\frac{kv_d}{\omega_p}\right)^2}\right)} \underset{kv_d \ll \omega_p}{\sim} \omega_p, \quad (52)$$



two another pure imaginary conjugate poles

$$\omega_{3/4}(k < k_c) = \pm i\delta(k). \quad (53)$$

It means that the two counter-propagating electron beams streaming through the immobile plasma ions are unstable on space scales greater than  $2\pi v_d/\omega_p$  and that this two-stream instability grows exponentially at the rate

$$\delta(k) = \omega_p \sqrt{\frac{1}{2} \left( \sqrt{1 + 8 \left( \frac{kv_d}{\omega_p} \right)^2} - 1 \right) - \left( \frac{kv_d}{\omega_p} \right)^2} \sim_{kv_d \ll \omega_p} |k| v_d. \quad (54)$$

The stable electron plasma waves angular frequency Equation 52 and the two stream instability growth rate Equation 54 are plotted in Figure 5 as a function of the angular spatial frequency mode  $k$ . Retaining the main terms in the series expansions of  $\mathcal{Z}$  up to the second order in Equation 45 according to Equation 49, the Fourier components of the electrostatic field Laplace transform simplify into

$$\widehat{\delta E}_{x,p}^{(+)}(\omega) \sim_{v_d \gg v_{Te0}} -\alpha_p A \frac{m_e v_d}{e} \frac{\omega_p^2}{\epsilon(\omega, k_p)(\omega - k_p v_d)(\omega + k_p v_d)}. \quad (55)$$

The poles of the Fourier components of the electrostatic fields Equation 55 are thus  $\pm k_p v_d$  plus the ones of the plasma electrical permittivity Equation 50 given by Equations 51 and Equation 53. We can now determine the time dependence of the spatial Fourier components of the growing electrostatic field

$$\widehat{\delta E}_{x,p}(t) = \frac{1}{2\pi} \int_{\iota R - \infty}^{\iota R + \infty} \widehat{\delta E}_{x,p}^{(+)}(\omega) \exp(+i\omega t) d\omega \quad (56)$$

by using the residue theorem with the contour illustrated in Figure 6 in order to evaluate the Cauchy principal value of this integral : since the function to integrate in Equation 56 is an analytic function of  $\omega$  defined in the whole complex plane, we moved the contour of integration usually taken slightly above the real axis into the lower half-plane sufficiently far beneath the pole  $-i\delta$  and passing round this pole and round the other poles lying above it in such a way that it doesn't cross any of the poles of the function. We thus obtain

$$\begin{aligned} \widehat{\delta E}_{x,p}(t) = & A E_0 \alpha_p \frac{\omega_p}{\delta(k_p)} \frac{\delta(k_p)^2 + (k_p v_d)^2}{\delta(k_p)^2 + \omega_0(k_p)^2} \sinh[\delta(k_p)t] \\ & + A \frac{E_0}{2} \alpha_p \frac{\omega_p}{\omega_0(k_p)} \frac{\omega_0(k_p)^2 - (k_p v_d)^2}{\delta(k_p)^2 + \omega_0(k_p)^2} \sin[\omega_0(k_p)t] \end{aligned} \quad (57)$$

with

$$E_0 = \frac{m_e v_d \omega_p}{e} \quad (58)$$

that finally gives according to the Fourier series expansion Equation 39

$$\begin{aligned} \delta E_x(x, t) = & A E_0 \frac{\omega_p}{\delta(k_1)} \frac{\delta(k_1)^2 + (k_1 v_d)^2}{\delta(k_1)^2 + \omega_0(k_1)^2} \sinh[\delta(k_1)t] \sin(k_1 x) \\ & + A \frac{E_0}{2} \frac{\omega_p}{\omega_0(k_1)} \frac{\omega_0(k_1)^2 - (k_1 v_d)^2}{\delta(k_1)^2 + \omega_0(k_1)^2} \sin[\omega_0(k_1)t] \sin(k_1 x). \end{aligned} \quad (59)$$

Knowing the electrostatic field Equation 59, one may also deduce the perturbed distribution

244 function according to Equation 37. It reads

$$\begin{aligned}\delta f_e(x, v_x, t) &= \delta f_e(x, v_x, t=0) + \frac{e}{m_e} \frac{df_e^{(0)}}{dv_x}(v_x) \int_0^t \delta E_x[x + v_x(\tau - t), \tau] d\tau \\ &= f_{e,+}^{(0)}(v_x) \left[ +A \sin(k_1 x) + \frac{v_d - v_x}{v_{Te0}^2} \frac{e}{m_e} \int_0^t \delta E_x[x + v_x(\tau - t), \tau] d\tau \right] \\ &+ f_{e,-}^{(0)}(v_x) \left[ -A \sin(k_1 x) - \frac{v_d + v_x}{v_{Te0}^2} \frac{e}{m_e} \int_0^t \delta E_x[x + v_x(\tau - t), \tau] d\tau \right].\end{aligned}\quad (60)$$

245 In the limit  $k_p v_d \ll \omega_p$ , they simplify into

$$\delta E_x(x, t) \underset{k_1 v_d \ll \omega_p}{\sim} A \frac{E_0}{2} \left[ \sin(\omega_p t) + 4 \frac{k_1 v_d}{\omega_p} \sinh(k_1 v_d t) \right] \sin(k_1 x) \quad (61)$$

246 and

$$\begin{aligned}\underset{k_1 v_d \ll \omega_p}{\sim} & A \frac{v_d}{1 - \left(\frac{k_1 v_x}{\omega_p}\right)^2} \left\{ \frac{e}{m_e} \int_0^t \delta E_x[x + v_x(\tau - t), \tau] d\tau \right. \\ & \left. \frac{k_1 v_x}{\omega_p} \sin(\omega_p t) \cos(k_1 x) - [\cos(\omega_p t) - 1] \sin(k_1 x) \right\} \\ + & A \frac{v_d}{1 + \left(\frac{v_x}{v_d}\right)^2} \left\{ -\frac{v_x}{v_d} \sinh(k_1 v_d t) \cos(k_1 x) + [\cosh(k_1 v_d t) - 1] \sin(k_1 x) \right\}.\end{aligned}\quad (62)$$

247 We thus deduce in this limit

$$\begin{aligned}\delta n_e(x, t) &= \int_{-\infty}^{\infty} \delta f_e(x, v_x, t) dv_x \\ &\underset{k_1 v_d \ll \omega_p}{\sim} -\frac{A}{2} Z n_i \frac{k_1 v_d}{\omega_p} \left[ \sin(\omega_p t) + 4 \frac{k_1 v_d}{\omega_p} \sinh(k_1 v_d t) \right] \cos(k_1 x)\end{aligned}\quad (63)$$

248 and

$$\begin{aligned}\delta v_e(x, t) &= \frac{1}{Z n_i} \int_{-\infty}^{\infty} v_x \delta f_e(x, v_x, t) dv_x \\ &\underset{k_1 v_d \ll \omega_p}{\sim} -\frac{A}{2} v_d \left[ (\cos(\omega_p t) - 1) + \left(2 \frac{k_1 v_d}{\omega_p}\right)^2 (\cosh(k_1 v_d t) - 1) \right] \sin(k_1 x).\end{aligned}\quad (64)$$

249 The first term in the square brackets

$$\begin{cases} \delta n_{\text{osc}}(x, t) \underset{k_1 v_d \ll \omega_p}{\sim} -\frac{A}{2} Z n_i \frac{k_1 v_d}{\omega_p} \sin(\omega_p t) \cos(k_1 x) \\ \delta v_{\text{osc}}(x, t) \underset{k_1 v_d \ll \omega_p}{\sim} -\frac{A}{2} v_d (\cos(\omega_p t) - 1) \sin(k_1 x) \\ \delta E_{\text{osc}}(x, t) \underset{k_1 v_d \ll \omega_p}{\sim} \frac{A}{2} E_0 \sin(\omega_p t) \sin(k_1 x) \end{cases} \quad (65)$$

250 corresponds to space-charge oscillations of stationary electrostatic plasma waves excited by  
251 the perturbation imposed on each electron beam. We are rather interested here in the second  
252 term in the square brackets

$$\begin{cases} \delta n_{\text{ins}}(x, t) \underset{k_1 v_d \ll \omega_p}{\sim} -2A Z n_i \left(\frac{k_1 v_d}{\omega_p}\right)^2 \sinh(k_1 v_d t) \cos(k_1 x) \\ \delta v_{\text{ins}}(x, t) \underset{k_1 v_d \ll \omega_p}{\sim} -2A v_d \left(\frac{k_1 v_d}{\omega_p}\right)^2 (\cosh(k_1 v_d t) - 1) \sin(k_1 x) \\ \delta E_{\text{ins}}(x, t) \underset{k_1 v_d \ll \omega_p}{\sim} 2A E_0 \frac{k_1 v_d}{\omega_p} \sinh(k_1 v_d t) \sin(k_1 x) \end{cases} \quad (66)$$

corresponding to the exponentially growing electrostatic field due to the two-stream instability. These latter growing electron density, current density and electrostatic field perturbations Equation 66 can directly be compared with the ESVM simulation result. One can also check that if  $A = 0$ , all quantities cancel. That confirms that, contrary to PIC codes, the two counter-propagating electron beams would continue their propagation without any modification if we do not impose an initial perturbation on which the instability will grow in ESVM. Finally, one can estimate the trajectories  $(x_\ell, v_\ell)$  of one beam electron  $\ell \in [1, N_e]$  with an arbitrary initial velocity  $v_\ell(t=0) = v_0$  in the beam velocity distribution function and an initial position  $x_\ell(t=0) = x_0$  close to  $x = 0$  such that  $k_1 x_0 \ll 1$ . At the early stage of the instability, the growing electrostatic field component  $\delta E_{\text{ins}}$  is small compared to the stationary plasma wave  $\delta E_{\text{osc}}$  that oscillates in time at the Langmuir electron angular frequency  $\omega_p$ . On such time scale  $\omega_p t \sim 1$ , the beam electrons are consequently mainly affected by this electrostatic field component

$$m_e \frac{dv_\ell}{dt} = -e\delta E_{\text{osc}}(x_\ell(t), t) \quad (67)$$

and their trajectory is thus given by

$$\frac{d^2 x_\ell}{dt^2} + \omega_p^2 \left( \frac{A k_1 v_d}{2 \omega_p} \right) \sin(\omega_p t) x_\ell(t) = 0, \quad (68)$$

assuming that  $k_1 x_\ell(t) \ll 1$  remains valid at every time  $t > 0$  if it is valid at  $t = 0$  such that  $\forall t, \sin[k_1 x_\ell(t)] \sim k_1 x_\ell(t)$ . Recognizing the Mathieu Equation

$$\frac{d^2 x_\ell}{du^2} + [a - 2q \cos(2u)] x_\ell(u) = 0 \quad (69)$$

with  $a = 0$  and  $q = -Ak_1 v_d / \omega_p$  by doing the change of variable  $u(t) = (-\pi/4) + (\omega_p t/2)$ , we deduce

$$k_1 x_\ell(t) = k_1 x_c c_{e,0}[q, u(t)] + k_1 x_s s_{e,0}[q, u(t)] \quad (70)$$

and

$$v_\ell(t) = \frac{v_d}{2} \frac{\omega_p}{k_1 v_d} \{k_1 x_c c'_{e,0}[q, u(t)] + k_1 x_s s'_{e,0}[q, u(t)]\} \quad (71)$$

with

$$\begin{cases} k_1 x_c = + \frac{s'_{e,0}(q, -\pi/4) k_1 x_0 - s_{e,0}(q, -\pi/4) (2k_1 v_d / \omega_p) (v_0 / v_d)}{c_{e,0}(q, -\pi/4) s'_{e,0}(q, -\pi/4) - c'_{e,0}(q, -\pi/4) s_{e,0}(q, -\pi/4)} \\ k_1 x_s = - \frac{c'_{e,0}(q, -\pi/4) k_1 x_0 - c_{e,0}(q, -\pi/4) (2k_1 v_d / \omega_p) (v_0 / v_d)}{c_{e,0}(q, -\pi/4) s'_{e,0}(q, -\pi/4) - c'_{e,0}(q, -\pi/4) s_{e,0}(q, -\pi/4)} \end{cases}, \quad (72)$$

accounting for the initial conditions at  $t = 0$ . Here,  $c_{e,a}(q, u)$  and  $s_{e,a}(q, u)$  are respectively the even and odd solutions of Mathieu Equation Equation 69 and  $c'_{e,a}(q, u)$  and  $s'_{e,a}(q, u)$  their first order derivatives. According to Equation 70 and Equation 71, the beam electron trajectories in space are only slightly modified compared to their ballistic initial trajectory  $x_0 + v_0 t$  with a velocity that oscillates around their initial value  $v_0$  with amplitudes slightly increasing with time. As a consequence, each beam velocity dispersion slightly increases with its propagation distance until the growing component of the electrostatic field  $\delta E_{\text{ins}}$  becomes greater than  $\delta E_{\text{osc}}$ . When this occurs, the equation of motion

$$m_e \frac{dv_\ell}{dt} = -e\delta E_{\text{ins}}(x_\ell(t), t) \quad (73)$$

gives

$$\frac{1}{2} \left( \frac{v_\ell(t)}{v_d} \right)^2 - \frac{1}{2} \left( \frac{v_0}{v_d} \right)^2 = -2Ak_1 \int_0^t v_\ell(t) \sin[k_1 x_\ell(t)] \sinh(k_1 v_d t) dt \quad (74)$$

and

$$\frac{d^2 x_\ell}{dt^2} + 2k_1 v_d^2 \sinh(k_1 v_d t) \sin[k_1 x_\ell(t)] = 0. \quad (75)$$

The energy conservation Equation Equation 74 shows that, at the early stage of the instability, electrons having a positive velocity  $v_\ell(t) > 0$  at a location  $0 < x_\ell(t) < L_x/2$  as well as electrons having a negative velocity  $v_\ell(t) < 0$  at a location  $-L_x/2 < x_\ell(t) < 0$  are losing energy contrary to electrons having a negative velocity  $v_\ell(t) < 0$  at a location  $0 < x_\ell(t) < L_x/2$  or electrons having a positive velocity  $v_\ell(t) > 0$  at a location  $-L_x/2 < x_\ell(t) < 0$  that are earning energy. In order to determine such an electron trajectory according to its equation of motion Equation 75, one can assume in addition that  $k_1 x_\ell(t) \ll 1$  remains valid at every time  $t > 0$  if it is valid at  $t = 0$  such that  $\forall t, \sin[k_1 x_\ell(t)] \sim k_1 x_\ell(t)$  and consider time scales of the order of electrostatic plasma oscillations  $\omega_p^{-1}$  so that we may consider  $\sinh(k_1 v_d t) \sim \exp(k_1 v_d t)/2$ . In this case, Equation 75 simplifies into

$$\frac{d^2 x_\ell}{dt^2} + (k_1 v_d)^2 \exp(k_1 v_d t) x_\ell(t) = 0. \quad (76)$$

Recognizing the differential Bessel Equation by doing the change of variable  $v(t) = \exp(k_1 v_d t)$

$$\frac{d^2 x_\ell}{dv^2} + \frac{1}{v} \frac{dx_\ell}{dv} + \frac{1}{v} x_\ell(v) = 0, \quad (77)$$

the beam electron trajectories can be found readily. They read

$$k_1 x_\ell(t) = k_1 x_J J_0(2\sqrt{v(t)}) + k_1 x_Y Y_0(2\sqrt{v(t)}) \quad (78)$$

and

$$v_\ell(t) = -v_d \left[ k_1 x_J J_1(2\sqrt{v(t)}) + k_1 x_Y Y_1(2\sqrt{v(t)}) \right] \sqrt{v(t)} \quad (79)$$

with

$$\begin{cases} k_1 x_J = + \frac{Y_1(2) k_1 x_0 + Y_0(2) (v_0/v_d)}{J_0(2) Y_1(2) - J_1(2) Y_0(2)} \\ k_1 x_Y = - \frac{J_1(2) k_1 x_0 + J_0(2) (v_0/v_d)}{J_0(2) Y_1(2) - J_1(2) Y_0(2)} \end{cases}, \quad (80)$$

accounting for the initial conditions at  $t = 0$ . Here,  $J_\mu$  and  $Y_\mu$  are the Bessel functions of the first and second kind of order  $\mu$  respectively. Some of these beam electron orbits are plotted in Figure 7. We can see that the beam electrons are looping around the phase-space center  $(x, v) = (0, 0)$  with a velocity amplitude increasing with their initial spatial distance from  $x = 0$  in agreement with the ESVM simulation Figure 4.

## ESVM Perspectives

It is planned in a near future to : 1) provide another Plasma Physics academic simulation about one BGK (from the name of its finder I. B. Bernstein, J. M. Greene and M. D. Kruskal) non linear electron plasma wave (Bernstein et al., 1957) 2) provide another Plasma Physics academic simulation about Plasma wave echo (Gould et al., 1967) 3) implement non-equally spaced phase-space cells 4) implement high order Weighted Essentially Non-Oscillatory (WENO) advection schemes (Liu et al., 1994) 5) compute the plasma ion Vlasov equation to allow for the ions to be mobile 6) implement MPI parallelization 7) implement vectorization 8) store the simulation results in hdf5 files instead of text files 9) extend the code to the relativistic regime : ESVM  $\Rightarrow$  RESVM for open source Relativistic ElectroStatic Vlasov-Maxwell code 10) implement a BGK (from the name of its finder P. L. Bhatnagar, E. P. Gross and M. Krook) collision operator (Bhatnagar et al., 1954) 11) extend the code to 1D-2V and 1D-3V phase-space electrostatic plasma simulations 12) implement the Landau (Landau, 1937) and Belaiev-Budker (Belaiev & Budker, 1956) relativistic collision operators using the Rosenbluth potentials (Rosenbluth et al., 1957) and their relativistic Braams-Karney extension (Braams & Karney, 1987) : (R)ESVM  $\Rightarrow$  (R)EMVFPM for open source (Relativistic) ElectroMagnetic Vlasov-Fokker-Planck-Maxwell code 13) extend the code to electromagnetic 2D-1V, 2D-2V and 2D-3V phase-space electrostatic electromagnetic plasma simulations

321 : (R)ESVM/(R)EMVM  $\Rightarrow$  (R)ESVM2/(R)EMVM2 and (R)ESVFPM2/(R)EMVFPM2 for  
 322 open source (Relativistic) ElectroStatic/ElectroMagnetic Vlasov-Maxwell and Vlasov-Fokker-  
 323 Planck-Maxwell in 2D 14) implement the Perfectly Matched Layer (PML) technique (Berenger,  
 324 1994) to absorb the electromagnetic fields at the spatial simulation box boundaries 15) deploy  
 325 the code to GPU architectures.

## 326 Figures

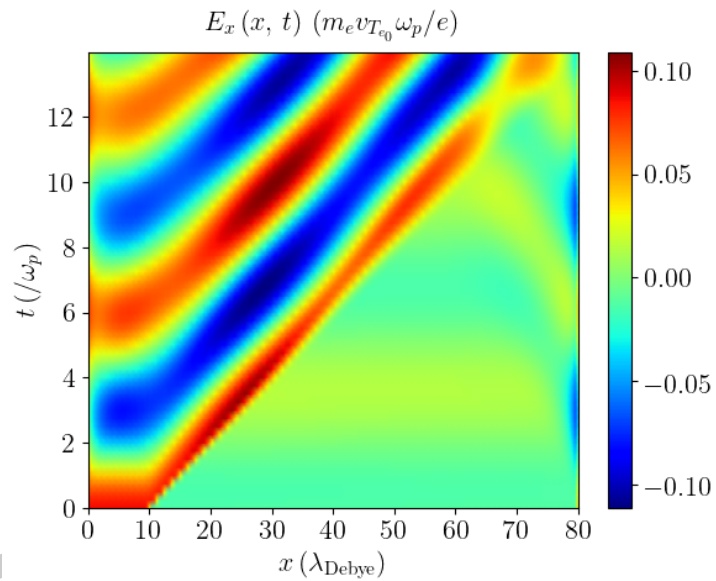


**Figure 1:** Electrostatic wakefield test case : Electrostatic wakefield  $E_x(x, t)$  emitted by a Gaussian electron propagating in a collisionless plasma at Maxwell-Boltzmann equilibrium Equation 27 and initialized according to Equation 28 with  $A = 0.1$  and  $\underline{v_d} = 5$ .

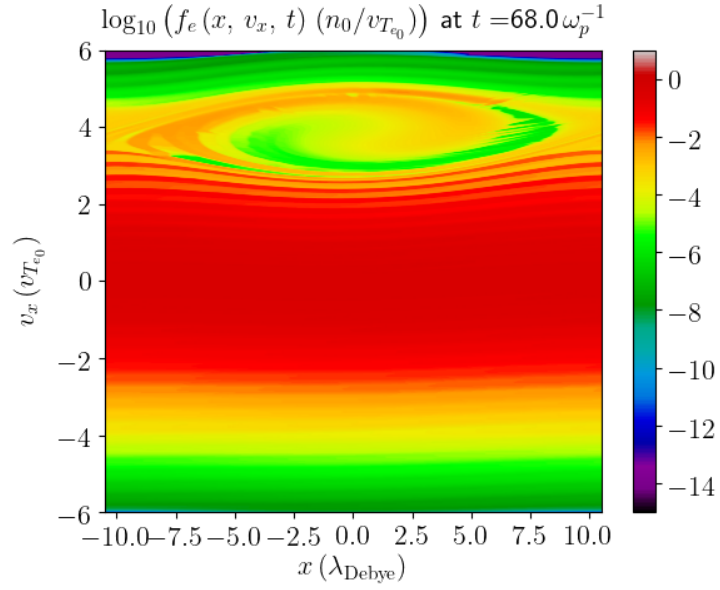


**Figure 2:** Non Linear Landau damping test case : Plasma electrons phase-space  $f_e(x, v_x, t = 68)$  in the non-linear Landau damping of the electron plasma wave propagating in the collisionless plasma at Maxwell-Boltzmann equilibrium Equation 27 and initialized according to Equation 29 with  $A = 10^{-1}$ ,  $\underline{k} = 0.29919930034$  and  $\underline{\omega}_0 = 1.18$ .

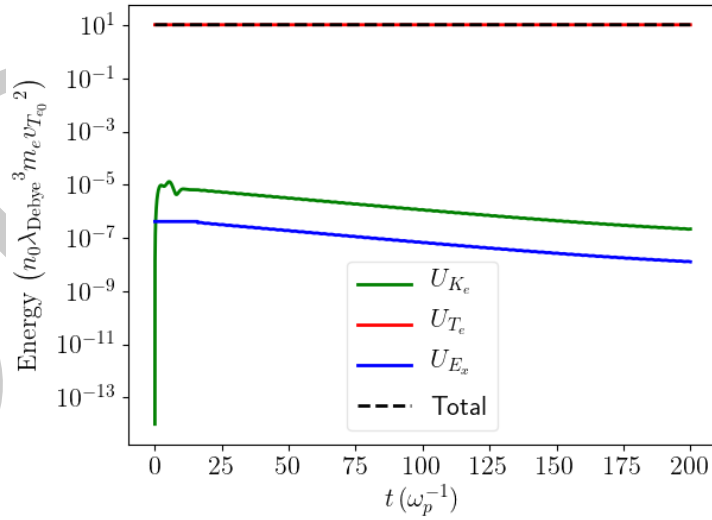


**Figure 3:** Linear Landau damping test case : Total electrostatic field energy and plasma electrons kinetic energy time evolution of the linearly Landau damped electron plasma wave propagating in the collisionless plasma at Maxwell-Boltzmann equilibrium Equation 27 and initialized according to Equation 29 with  $A = 10^{-3}$ ,  $\underline{k} = 0.29919930034$  and  $\underline{\omega}_0 = 1.18$ .

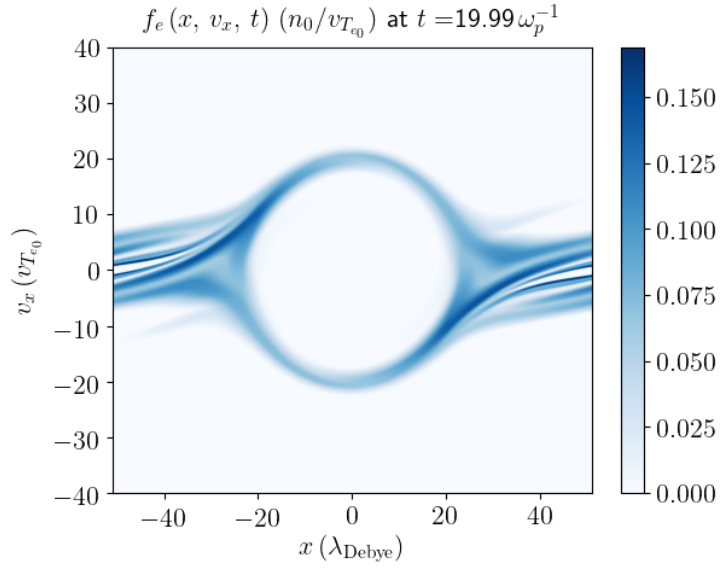


**Figure 4:** Two stream instability test case : Plasma electrons phase-space  $f_e(\underline{x}, v_x, \underline{t} = 19.99)$  in the two-stream instability of two counter-propagating electron beams initialized according to Equation 34 with  $A = 10^{-1}$ ,  $\underline{k} = 0.06159985595$  ( $x_{\min} = -x_{\max} = 51$ ) and  $v_d = 10$ .

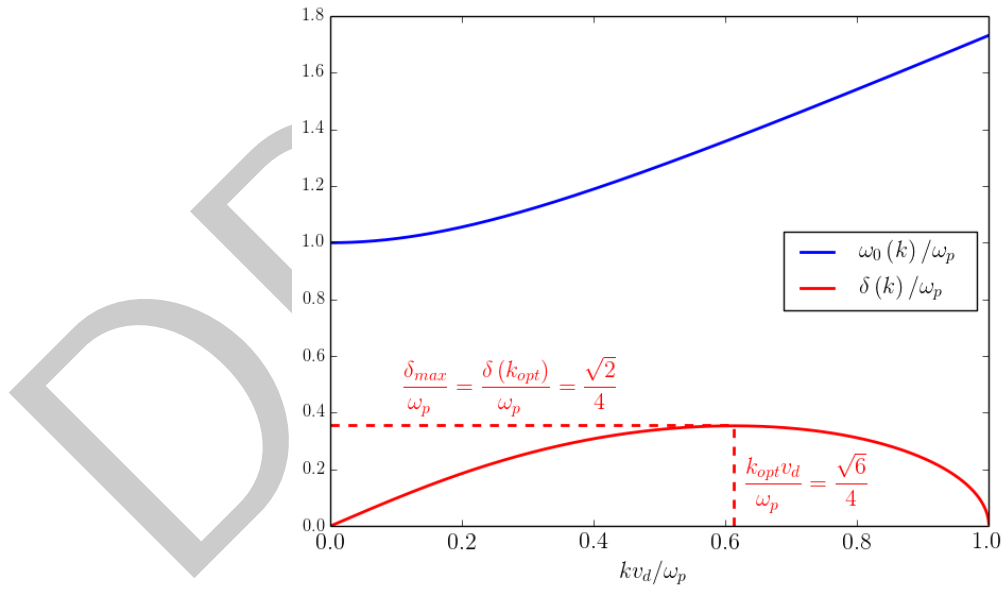


**Figure 5:** Two stream instability test case : Stationary electron plasma waves angular frequency Equation 52 seeded by the perturbation Equation 35 and the two-stream instability growth rate Equation 54 as a function of the spatial angular frequency mode  $k$ .



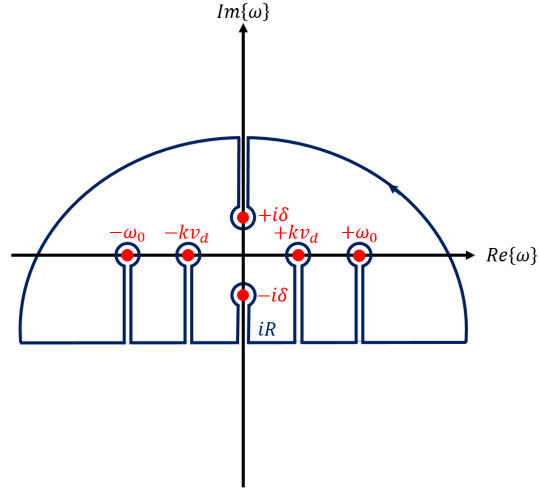


**Figure 6:** Two stream instability test case : Integration contour used to evaluate the the Cauchy principal value of the integral Equation 56.

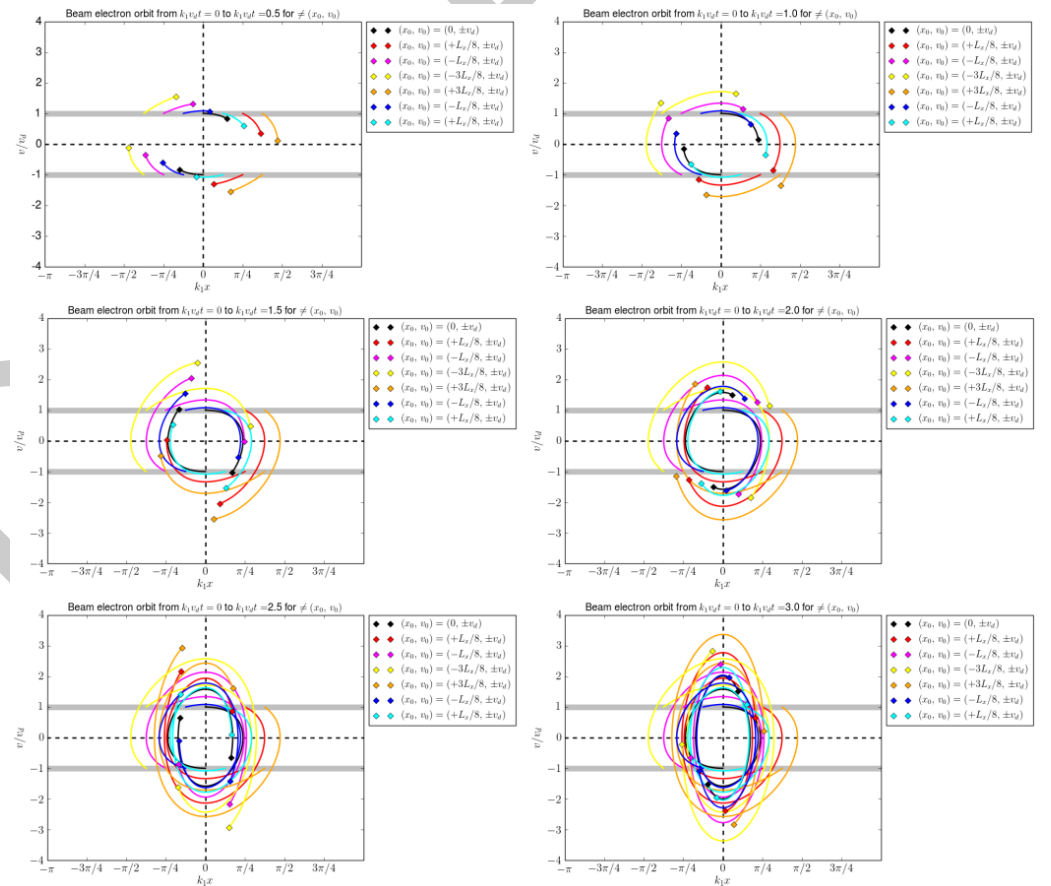


**Figure 7:** Two stream instability test case : Some beam electron orbits according to analytical estimates Equation 78 and Equation 79.

## References

- Beam, R. M., & Warming, R. F. (1976). An implicit finite-difference algorithm for hyperbolic systems in conservation-law form. *Journal of Computational Physics*, 22(1), 87–110. [https://doi.org/https://doi.org/10.1016/0021-9991\(76\)90110-8](https://doi.org/https://doi.org/10.1016/0021-9991(76)90110-8)
- Belaiev, S. T., & Budker, G. I. (1956). *Dokl. Akad. Nauk SSSR*, 107.
- Berenger, J.-P. (1994). A perfectly matched layer for the absorption of electromagnetic waves. *Journal of Computational Physics*, 114(2), 185–200. <https://doi.org/https://doi.org/10.1006/jcph.1994.1159>
- Bernstein, I. B., Greene, J. M., & Kruskal, M. D. (1957). Exact nonlinear plasma oscillations. *Phys. Rev.*, 108, 546–550. <https://doi.org/https://doi.org/10.1103/PhysRev.108.546>
- Bhatnagar, P. L., Gross, E. P., & Krook, M. (1954). A model for collision processes in gases. I. Small amplitude processes in charged and neutral one-component systems. *Phys. Rev.*, 94, 511–525. <https://doi.org/https://doi.org/10.1103/PhysRev.94.511>
- Braams, B. J., & Karney, C. F. F. (1987). Differential form of the collision integral for a relativistic plasma. *Phys. Rev. Lett.*, 59, 1817–1820. <https://doi.org/https://doi.org/10.1103/PhysRevLett.59.1817>
- Courant, R., Friedrichs, K., & Lewy, H. (1928). Über die partiellen differenzengleichungen der mathematischen. *Physik. Math. Ann.*, 100, 32–74. <https://doi.org/https://doi.org/10.1007/BF01448839>
- Courant, R., Isaacson, E., & Rees, M. (1952). On the solution of nonlinear hyperbolic differential equations by finite differences. *Communications on Pure and Applied Mathematics*, 5(3), 243–255. <https://doi.org/https://doi.org/10.1002/cpa.3160050303>
- Crouseilles, N., & Filbet, F. (2004). Numerical approximation of collisional plasmas by high order methods. *Journal of Computational Physics*, 201(2), 546–572. <https://doi.org/https://doi.org/10.1016/j.jcp.2004.06.007>
- Dawson, J. (1962). One-dimensional plasma model. *The Physics of Fluids*, 5(4), 445–459. <https://doi.org/https://doi.org/10.1063/1.1706638>
- de Buyl, P. (2014). The vmf90 program for the numerical resolution of the vlasov equation for mean-field systems. *Computer Physics Communications*, 185(6), 1822–1827. <https://doi.org/https://doi.org/10.1016/j.cpc.2014.03.004>
- Decyk, V. K. (1987). Simulation of microscopic processes in plasma. *Proc. 1987 International Conference on Plasma Physics, Kiev, USSR, April 1987, Ed. A G Sitenko [World Scientific, Singapore, 1987] Vol. II, p. 1075.*
- Deroouillat, J., Beck, A., Pérez, F., Vinci, T., Chiamello, M., Grassi, A., Flé, M., Bouchard, G., Plotnikov, I., Aunai, N., Dargent, J., Riconda, C., & Grech, M. (2018). Smilei : A collaborative, open-source, multi-purpose particle-in-cell code for plasma simulation. *Computer Physics Communications*, 222, 351–373. <https://doi.org/https://doi.org/10.1016/j.cpc.2017.09.024>
- Duclous, R., Dubroca, B., Filbet, F., & Tikhonchuk, V. (2009). High order resolution of the maxwell-fokker-planck-landau model intended for ICF applications. *Journal of Computational Physics*, 228(14), 5072–5100. <https://doi.org/https://doi.org/10.1016/j.jcp.2009.04.005>
- Fried, B. D., & Conte, S. D. (1961). Elsevier.
- Fromm, J. E. (1968). A method for reducing dispersion in convective difference schemes. *Journal of Computational Physics*, 3(2), 176–189. [https://doi.org/https://doi.org/10.1016/0021-9991\(68\)90015-6](https://doi.org/https://doi.org/10.1016/0021-9991(68)90015-6)

- 373 Godunov, S. K. (1959). Eine differenzenmethode für die näherungsberechnung unstetiger  
374 lösungen der hydrodynamischen gleichungen. *Mat. Sb., Nov. Ser.*, 47, 271–306.
- 375 Gould, R. W., O'Neil, T. M., & Malmberg, J. H. (1967). Plasma wave echo. *Phys. Rev.*  
376 *Lett.*, 19, 219–222. <https://doi.org/10.1103/PhysRevLett.19.219>
- 377 Joglekar, A. S., & Levy, M. C. (2020). VlaPy: A python package for eulerian vlasov-poisson-  
378 fokker-planck simulations. *Journal of Open Source Software*, 5(53), 2182. [https://doi.](https://doi.org/10.21105/joss.02182)  
379 [org/10.21105/joss.02182](https://doi.org/10.21105/joss.02182)
- 380 Landau, L. D. (1937). *JETP*, 7, 203.
- 381 Landau, L. D., & Lifshitz, E. M. (1981). *Physical kinetics* (Vol. 10). Pergamon Press.
- 382 Lax, P., & Wendroff, B. (1960). Systems of conservation laws. *Communications on Pure*  
383 *and Applied Mathematics*, 13(2), 217–237. [https://doi.org/https://doi.org/10.1002/cpa.](https://doi.org/10.1002/cpa.3160130205)  
384 [3160130205](https://doi.org/10.1002/cpa.3160130205)
- 385 Liu, X.-D., Osher, S., & Chan, T. (1994). Weighted essentially non-oscillatory schemes.  
386 *Journal of Computational Physics*, 115(1), 200–212. [https://doi.org/https://doi.org/10.](https://doi.org/10.1006/jcph.1994.1187)  
387 [1006/jcph.1994.1187](https://doi.org/10.1006/jcph.1994.1187)
- 388 Roe, P. L. (1986). Characteristic-based schemes for the euler equations. *Annual Review of*  
389 *Fluid Mechanics*, 18(1), 337–365. <https://doi.org/10.1146/annurev.fl.18.010186.002005>
- 390 Rosenbluth, M. N., MacDonald, W. M., & Judd, D. L. (1957). Fokker-planck equation for  
391 an inverse-square force. *Phys. Rev.*, 107, 1–6. <https://doi.org/10.1103/PhysRev.107.1>
- 392 Sagdeev, R. Z., & Galeev, A. A. (1969). *Nonlinear Plasma Theory*. W. A. Benjamin, Inc.,  
393 New York.
- 394 Touati, M., Feugeas, J.-L., Nicolai, P., Santos, J. J., Gremillet, L., & Tikhonchuk, V. T.  
395 (2014). A reduced model for relativistic electron beam transport in solids and dense  
396 plasmas. *New Journal of Physics*, 16(7), 073014. [https://doi.org/10.1088/1367-2630/](https://doi.org/10.1088/1367-2630/16/7/073014)  
397 [16/7/073014](https://doi.org/10.1088/1367-2630/16/7/073014)
- 398 Tzoufras, M., Bell, A. R., Norreys, P. A., & Tsung, F. S. (2011). A vlasov-fokker-planck code  
399 for high energy density physics. *Journal of Computational Physics*, 230(17), 6475–6494.  
400 [https://doi.org/https://doi.org/10.1016/j.jcp.2011.04.034](https://doi.org/10.1016/j.jcp.2011.04.034)
- 401 van Leer, B. (1979). Towards the ultimate conservative difference scheme. V. A second-  
402 order sequel to godunov's method. *Journal of Computational Physics*, 32(1), 101–136.  
403 [https://doi.org/https://doi.org/10.1016/0021-9991\(79\)90145-1](https://doi.org/10.1016/0021-9991(79)90145-1)
- 404 Van Leer, B. (1977). Towards the ultimate conservative difference scheme III. Upstream-  
405 centered finite-difference schemes for ideal compressible flow. *Journal of Computational*  
406 *Physics*, 23(3), 263–275. [https://doi.org/https://doi.org/10.1016/0021-9991\(77\)](https://doi.org/10.1016/0021-9991(77)90094-8)  
407 [90094-8](https://doi.org/10.1016/0021-9991(77)90094-8)
- 408 Yee, K. (1966). *IEEE Transactions on Antennas and Propagation*, 14(3), 302–307. <https://doi.org/10.1109/TAP.1966.1138693>  
409